Syntheses, Structure, Magnetism, and Optical Properties of the Partial Ordered Quaternary Interlanthanide Sulfides $PrLnYb_2S_6$ (Ln = Tb, Dy)

Geng Bang Jin,[†] Eun Sang Choi,[‡] Robert P. Guertin,[§] James S. Brooks,[‡] Travis H. Bray,[†] Corwin H. Booth,[£] and Thomas E. Albrecht-Schmitt[†,*]

[†]Department of Chemistry and Biochemistry and the E. C. Leach Nuclear Science Center, Auburn University, Auburn, Alabama 36849

[‡]Department of Physics and National High Magnetic Field Laboratory, Florida State University, Tallahassee, Florida 32310

[§]Department of Physics and Astronomy, Tufts University, Medford, Massachusetts 02155

[£]Chemical Sciences Division, Lawrence Berkeley National Laboratory, 1 Cyclotron Rd., Berkeley, CA 94720

Published in J. Solid State Chem. ***180****, 2581 (2007).*

Abstract

Dark red single crystals of $PrLnYb_2S_6$ (Ln = Pr/Yb, Tb, Dy) have been synthesized through the reaction of elemental rare earth metals and S using a Sb_2S_3 flux at 1000 °C. These isotypic compounds adopt the F-Ln_2S_3 three-dimensional open channel structure type. Eight-coordinate Pr^{3+} ions sit in the channels, which are constructed from three different edge-shared double chains running down the *b* axis, which contain $Yb(1)S_6$ octahedra, $Yb(2)S_6$, octahedra and LnS_7 monocapped trigonal prisms, respectively. Each double chain connects to four other neighbors by sharing vertices and edges. Considerable disordering in Ln positions was observed in single X-ray diffraction experiments only in the case of Pr/Yb. Least square refinements gave rise to the formulas of $Pr_{1.34}Yb_{2.66}S_6$, of $PrTbYb_2S_6$, and $PrDyYb_2S_6$, which are confirmed by the elemental analysis and magnetic susceptibility measurements. $Pr_{1.34}Yb_{2.66}S_6$, $PrTbYb_2S_6$ and $PrDyYb_2S_6$ are paramagnetic down to 2 K without any indications of long range magnetic ordering. The optical transitions for $Pr_{1.34}Yb_{2.66}S_6$, $PrTbYb_2S_6$, and $PrDyYb_2S_6$ are at approximately 1.6 eV.Crystallographic data: $Pr_{1.34}Yb_{2.66}S_6$, monoclinic, space group $P2_1/m$, a = 10.960(2), b = 3.9501(8), c = 11.220(2) Å, β = 108.545(3), V = 460.54(16), Z = 2; $PrTbYb_2S_6$, monoclinic, space group $P2_1/m$, a = 10.9496(10), b = 3.9429(4), c = 11.2206(10) Å, β = 108.525(2), V = 459.33(7), Z = 2; $PrDyYb_2S_6$, monoclinic, space group $P2_1/m$, a = 10.9384(10), b = 3.9398(4), c = 11.2037(10) Å, β = 108.612(2), V = 457.57(7), Z = 2.

Introduction

There have been numerous studies on ternary interlanthanide chalcogenides in terms of their diverse structural chemistry and interesting physical properties [1-18]. α-$LnLn'S_3$ [1-4] ($GdFeO_3$ type [19]), $CeYb_3S_6$ [5,6] (F-Ln_2S_3 type [20,21]), $Sc_2Er_3S_7$ [7] (Y_5S_7 type [22]) and $EuLn_2Q_4$ [8-10] ($CaFe_2O_4$ type [23]) possess three-dimensional open channel structures, wherein the larger Ln^{3+} ions sit in the channels formed by smaller lanthanide chalcogenides polyhedra. While β-$LnLn'Q_3$ (Q = S, Se) [3,11,12] ($UFeS_3$ type [24]), and γ-$LnLn'S_3$ (Ln = La, Ce; Ln' = Er, Tm, Yb) [13] have layers of $Ln'Q_x$ polyhedra, separated by larger Ln^{3+} ions. δ-$LnLuS_3$ (Ln = Ce, Pr, Nd) [14] ($CeTmS_3$ type [15]) have a very condensed three-dimensional structure. Recent work has shown that the electronic and magnetic properties of these materials highly depend on the structures they adopt and the choices of lanthanides. For example, the optical band gap of γ-$LnLn'S_3$ (Ln = La, Ce; Ln' = Er, Tm, Yb) [13] are approximately 1.3 – 1.6 eV, while $SmEr_3S_6$ is 2.4 – 2.6 eV [16]. δ-$LnLuS_3$ (Ln = Pr, Nd) exhibit possible short-range antiferromagnetic ordering at low temperatures [14].

In contrast, there are no existing ordered quaternary interlanthanide chalcogenides that possess three different lanthanide elements. Instead of making new ordered quaternary phases, they can be prepared using intermediate lanthanides to substitute in the disordered sites in already known ternary structures. F-Ln_2S_3 type [17,18] ternary compounds are probably the best candidates to achieve this goal. This structure type has three different coordination environments for Ln^{3+} as octahedral, and mono- and bicapped prisms. The seven-coordinate sites are often disordered. By carefully choosing three different metals, ordered quaternary phases can be accessed. In this paper, we present the syntheses, structure, optical and magnetic properties of

first two partial ordered quaternary interlanthanide chalcogenides, $PrTbYb_2S_6$ and $PrDyYb_2S_6$. As a reference, $Pr_{1.34}Yb_{2.66}S_6$ is also included in the discussion.

Experimental

Starting Materials. Pr (99.9%, Alfa-Aesar), Tb (99.9%, Alfa-Aesar), Dy (99.9%, Alfa-Aesar), Yb (99.9%, Alfa-Aesar), S (99.5%, Alfa-Aesar), and Sb (99.5%, Alfa-Aesar) were used as received. The Sb_2S_3 flux was prepared from the direct reaction of the elements in sealed fused-silica ampoules at 850 °C.

Syntheses. $PrLnYb_2S_6$ (Ln = Tb, Dy) were prepared through the reaction of Pr (0.17 mmol), Ln (0.17 mmol), Yb (0.34 mmol), S (1.02 mmol), and Sb_2S_3 (0.17 mmol). For $Pr_{1.34}Yb_{2.66}S_6$, the reaction mixture consists of Pr (0.23 mmol), Yb (0.45 mmol), S (1.02 mmol), and Sb_2S_3 (0.17 mmol). All of the reactants were loaded into fused-silica ampoules under an argon atmosphere in a glovebox. The ampoules were sealed under vacuum and heated in a programmable tube furnace. The following heating profile was used: 2 °C/min to 500 °C (held for 1 h), 0.5 °C/min to 1000 °C (held for 5 d), 0.04 °C/min to 550 °C (held for 2 d), and 0.5 °C/min to 24 °C. Powder X-ray diffraction measurements were used to confirm phase purity by comparing the powder patterns calculated from the single crystal X-ray structures with the experimental data. Semi-quantitative SEM/EDX analyses were performed using a JEOL 840/Link Isis or JEOL JSM-7000F instruments. Pr, Ln, Yb, and S percentages were calibrated against standards. Sb was not detected in the crystals. Pr:Ln:Yb:S ratios of close to 1:1:2:6 were found for $PrLnYb_2S_6$ (Ln = Tb, Dy), while the Pr:Yb:S ratios in $Pr_{1.34}Yb_{2.66}S_6$ samples are approximately 2:1:4.5 from EDX analyses.

Crystallographic Studies. Single crystals of $PrLnYb_2S_6$ (Ln = Pr/Yb, Tb, Dy) were mounted on glass fibers with epoxy and optically aligned on a Bruker APEX single crystal X-ray

diffractometer using a digital camera. Initial intensity measurements were performed using graphite monochromated Mo Kα (λ = 0.71073 Å) radiation from a sealed tube and monocapillary collimator. SMART (v 5.624) was used for preliminary determination of the cell constants and data collection control. The intensities of reflections of a sphere were collected by a combination of 3 sets of exposures (frames). Each set had a different ϕ angle for the crystal and each exposure covered a range of 0.3° in ω. A total of 1800 frames were collected with exposure times per frame of 10 or 20 seconds depending on the crystal.

For $PrLnYb_2S_6$ (Ln = Pr/Yb, Tb, Dy), determination of integrated intensities and global refinement were performed with the Bruker SAINT (v 6.02) software package using a narrow-frame integration algorithm. These data were treated first with a face-index numerical absorption correction using XPREP [25], followed by a semi-empirical absorption correction using SADABS [26]. The program suite SHELXTL (v 6.12) was used for space group determination (XPREP), direct methods structure solution (XS), and least-squares refinement (XL) [25]. The final refinements included anisotropic displacement parameters for all atoms and secondary extinction. Some crystallographic details are given in Table 1. Atomic coordinates and equivalent isotropic displacement parameters for $PrLnYb_2S_6$ (Ln = Pr/Yb, Tb, Dy) are given in Table 2-4. Additional crystallographic details can be found in the Supporting Information.

The formula of F-Ln_2S_3 type compounds can be expressed as $(A^{VIII})(B^{VII})(C^{VI})_2S_6$. In the case of $Pr_{1.34}Yb_{2.66}S_6$, eight-coordinate A sites were assigned as Pr atoms and both of seven-coordinate B and octahedral C positions were named as Yb at the beginning of the refinement. However the average bond distance of YbS_7 is longer than the accepted value, according to Shannon's radii data [27], and its thermalparameter is larger than the other Yb atoms. The elementary analysis showed that the ratio of Pr:Yb is 1:2. All of these evidences suggest that

there should be certain amount of disordering on B sites. The refinement of occupancy lowered the residual and weighting scheme and give rise to the final formula of $Pr_{1.34(1)}Yb_{2.66(1)}S_6$.

For $PrLnYb_2S_6$ (Ln = Tb, Dy), Pr, Ln, Yb atoms were put in A, B, and C positions respectively. This gave excellent residuals in the refinements and the suggested formulas as $PrLnYb_2S_6$ (Ln = Tb, Dy) are consistent with the EDX results. Considering the similarity among Pr, Ln, and Yb, small amount of disordering on B and C, even A sites can not be excluded.

Powder X-ray Diffraction. Powder X-ray diffraction patterns were collected with a Rigaku Miniflex powder X-ray diffractometer using Cu Kα (λ = 1.54056 Å) radiation.

Magnetic Susceptibility Measurements. Magnetism data were measured on powders in gelcap sample holders with a Quantum Design MPMS 7T magnetometer/susceptometer between 2 and 300 K and in applied fields up to 7 T. DC susceptibility measurements were made under zero-field-cooled conditions with an applied field of 0.1 T. Susceptibility values were corrected for the sample diamagnetic contribution according to Pascal's constants [28] as well as for the sample holder diamagnetism. θ_p values were obtained from extrapolations from fits between 100 and 300 K.

UV-vis-NIR Diffuse Reflectance Spectroscopy. The diffuse reflectance spectra $PrLnYb_2S_6$ (Ln = Pr/Yb, Tb, Dy) were measured from 200 to 1500 nm using a Shimadzu UV3100 spectrophotometer equipped with an integrating sphere attachment. The Kubelka-Munk function was used to convert diffuse reflectance data to absorption spectra [29].

Results and discussion

Structures of $PrLnYb_2S_6$ (Ln = Pr/Yb, Tb, Dy)

The isotypic series of $PrLnYb_2S_6$ (Ln = Pr/Yb, Tb, Dy) have the F-Ln_2S_3 type structure with Pr^{3+} ions sitting on eight-coordinate positions, Ln^{3+} ions in seven-coordinate positions and Yb^{3+} ions occupying two octahedral sites. As shown in Figure 1, the structure of these compounds is constructed from three different edge-shared double chains running down the b axis, which contain $Yb(1)S_6$ octahedra, $Yb(2)S_6$ octahedra, and LnS_7 monocapped trigonal prisms, respectively. Each double chain connects to four other neighbors by sharing vertices and edges to form the channels where Pr^{3+} ions reside. For example, $Yb(1)S_6$ double chains are bound to two $Yb(2)S_6$ double chains via corner-sharing and two LnS_7 double chains via edge-sharing. The PrS_8 polyhedra can be viewed as a bicapped trigonal prism, which is shown in Figure 2.

Selected bond distances for $PrLnYb_2S_6$ (Ln = Pr/Yb, Tb, Dy) are listed in Table 5. Pr-S bond distances rang from 2.8755(19) Å to 3.0127 Å, which are comparable to Shannon's radii data of 2.966 Å [27]. The average bond distances for Pr/YbS_7, TbS_7, and DyS_7 are 2.807(2) Å, 2.800(2) Å, and 2.792(2) Å respectively. Compared to the accepted values for PrS_7 (2.89 Å), YbS_7 (2.765 Å), TbS_7 (2.82 Å), and DyS_7 (2.81 Å), they are all reasonable [27]. The bond distances for YbS_6 octahedra are in the range of 2.6134(14) Å and 2.759(2) Å.

Magnetic susceptibility

The magnetic susceptibilities for $PrLnYb_2S_6$ (Ln = Pr/Yb, Tb, Dy), in the range of 2-300 K, are presented in Figure 3- 5. There are no indications of long range magnetic orderings down to 2 K. $Pr_{1.34}Yb_{2.66}S_6$ deviates from the ideal Curie-Weiss law below 70 K due to crystal-field splitting of lanthanide ions. $PrTbYb_2S_6$ shows a pure Curie-Weiss paramagnetic behavior in the whole temperature range. While the $1/\chi$ plot for $PrDyYb_2S_6$ exhibits a deviation from the Curie-Weiss law and the onset of upward curvature at low temperature. This may indicate a short-range antiferromagnetic ordering, which has been observed in compound δ-$Pr_{1.29}Lu_{0.71}S_3$ [14] in

previous report. Table 6 shows the magnetic parameters for $PrLnYb_2S_6$ (Ln = Pr/Yb, Tb, Dy), which were obtained from fitting the data in the range of 100 K and 300 K into the Curie-Weiss law. All of compounds have negative value of θ_p, which indicates antiferromagnetic interactions between cations. The experimental effective magnetic moments for these compounds are close to the accepted values [30]. This provides further supporting evidence for the proposed formula from the single crystal X-ray experiments.

Optical properties

The UV-vis-NIR diffuse reflectance spectra of $PrLnYb_2S_6$ (Ln = Pr/Yb, Tb, Dy) are present in Figure 6. They are very similar to each other. This suggests that the substitutions using different lanthanides ions in seven-coordinate Ln positions hardly change the band structures near the Fermi level for $PrLnYb_2S_6$ (Ln = Pr/Yb, Tb, Dy). The optical transition is mainly contributed from the interactions among eight-coordinate Pr^{3+} cations, six-coordinate Yb^{3+} cations and S^{2-} anions. It is also possible that the 4f-band of Pr, Yb, Tb, and Dy lie deep in the valence band. So the optical transitions are determined by the same gap between the [S]3p valence band and 5d(6s) conduction band [31,32]. The band gaps of $PrLnYb_2S_6$ (Ln = Pr/Yb, Tb, Dy) are approximately 1.6 eV, which are consistent with the dark red color they possess. They are also close to the values we reported for γ-LnLn'S_3 (Ln = La, Ce; Ln' = Er, Tm, Yb) [13] and δ-$Ln_{2-x}Lu_xS_3$ (Ln = Ce, Pr, Nd; x = 0.67-0.71) [14].

Conclusions

First two partial ordered quaternary interlanthanide sulfides $PrLnYb_2S_6$ (Ln = Tb, Dy) were prepared and characterized. They adopt same F-Ln_2S_3 type structure as the parent disordered $Pr_{1.34}Yb_{2.66}S_6$ phase. All three compounds are paramagnetic in the range of 2 and 300

K. The UV-vis-NIR diffuse reflectance spectra show that these compounds have very similar electronic structures near the Fermi level with wide band gaps. The elemental analysis and magnetic susceptibility measurements are consistent with the proposed formula.

Acknowledgment. This work was supported by the U.S. Department of Energy under Grant DE-FG02-02ER45963 through the EPSCoR Program. Funds for purchasing the UV-vis-NIR spectrometer used in these studies were provided through the Chemical Sciences, Geosciences and Biosciences Division, Office of Basic Energy Sciences, Office of Science, Heavy Elements Program, U.S. Department of Energy under Grant DE-FG02-01ER15187. JSB and ESC acknowledge support from NSF-DMR 0203532. A portion of this work was performed at the National High Magnetic Field Laboratory, which is supported by the National Science Foundation Cooperative Agreement No. DMR-0084173, by the State of Florida, and by the Department of Energy.

References

[1] N. Rodier, P. Laruelle, C. R. Seances Acad. Sci. Ser. *C* 270 (1970) 2127.

[2] D.J.W. Ijdo, Acta Crystallogr. B36 (1980) 2403.

[3] N. Rodier, R. Julien, V. Tien, Acta Crystallogr. C 39 (1983) 670.

[4] K.-J. Range, A. Gietl, U. Klement, Z. Kristallogr. 207 (1993) 147.

[5] N. Rodier, R. L. Firor, V. Tien, M. Guittard, Mat. Res. Bull. 11 (1976) 1209.

[6] N. Rodier, V. Tien, C. R. Acad. Sc. Paris Serie C 279 (1974) 817.

[7] N. Rodier, P. Laruelle, Bull. Soc. fr. de Mineral. Cristallogr. 95 (1972) 548.

[8] F. Hulliger, O. Vogt, Phys. Lett. 21 (1966) 138.

[9] W. Lugscheider, H. Pink, K. Weber, W. Zinn, Zeitschrift fuer Angewandte Physik 30 (1970) 36.

[10] P. Lemoine, D. Carre, M.Guittard, Acta Crystallogr. C 41 (1985) 667.

[11] D. Carré, P. Laruelle, Acta Crystallogr. B30 (1974) 952.

[12] K. Mitchell, R. C. Somers, F. Q. Huang, J. A. Ibers, J. Solid State Chem. 177 (2004) 709.

[13] G. B. Jin, E. S. Choi, R. P. Guertin, J. S. Brooks, T. H. Bray, C. H. Booth, T. E. Albrecht-Schmitt, Chem. Mater. 19 (2007) 567.

[14] G. B. Jin, E. S. Choi, R. P. Guertin, J. S. Brooks, T. H. Bray, C. H. Booth, T. E. Albrecht-Schmitt, J. Solid State Chem. in press.

[15] N. Rodier, Bull. Soc. fr. de Mineral. Cristallogr. 96 (1973) 350.

[16] Danielle L. Gray, Brandon A. Rodriguez, George H. Chan, Richard P. Van Duyne and James A. Ibers, J. Solid State Chem. in press.

[17] D. Carré, P. Laruelle, Acta Crystallogr. B29 (1973) 70.

[18] N. Rodier, V. Tien, Bull. Soc. fr. de Mineral. Cristallogr. 98 (1975) 30.

[19] M. Marezio, J.P. Remeika, P.D. Dernier, Acta Crystallogr. B26 (1970) 2008.

[20] T. Schleid, F. Lissner, J. Alloys Compd. 189 (1992) 69.

[21] C. M. Fang, A. Meetsma, G. A. Wiegers, J. Alloys Compd. 201 (1993) 255.

[22] C. Adolphe, Annales de Chimie (Paris), (1965) 271.

[23] D. F. Becker, J. S. Kasper, Acta Crystallogr. 10 (1957) 332.

[24] H. Noël, J. Padiou, Acta Crystallogr. B32 (1976) 1593.

[25] G. M. Sheldrick, SHELXTL PC, Version 6.12, An Integrated System for Solving, Refining, and Displaying Crystal Structures from Diffraction Data; Siemens Analytical X-Ray Instruments, Inc.: Madison, WI 2001.

[26] G. M. Sheldrick, *SADABS* 2001, Program for absorption correction using SMART CCD based on the method of Blessing: Blessing, R. H. Acta Crystallogr. A51 (1995) 33.

[27] R. D. Shannon, Acta Crystallogr. A32 (1976) 751.

[28] L. N. Mulay, E. A. Boudreaux, Theory and Applications of Molecular Diamagnetism, Wiley–Interscience: New York, 1976.

[29] W. W. Wendlandt, H. G. Hecht, Reflectance Spectroscopy, Interscience Publishers, New York, 1966.

[30] C. Kittel, Introduction to Solid State Physics, 6th Edition, Wiley, New York, (1986).

[31] A. V. Prokofiev, A. I. Shelykh, A. V. Golubkov, I. A. Smirnov, J. Alloys Compd. 219 (1995) 172.

[32] A. V. Prokofiev, A. I. Shelykh, B. T. Melekh, J. Alloys Compd. 242 (1996) 41.

Table 1. Crystallographic Data for $PrLnYb_2S_6$ (Ln = Pr/Yb, Tb, Dy).

Formula	$Pr_{1.34}Yb_{2.66}S_6$	$PrTbYb_2S_6$	$PrDyYb_2S_6$
fw	841.31	838.27	841.85
Color	dark red	dark red	dark red
Crystal System	monoclinic	monoclinic	monoclinic
Space group	$P2_1/m$ (No. 11)	$P2_1/m$ (No. 11)	$P2_1/m$ (No. 11)
a (Å)	10.960(2)	10.9496(10)	10.9384(10)
b (Å)	3.9501(8)	3.9429(4)	3.9398(4)
c (Å)	11.220(2)	11.2206(10)	11.2037(10)
β	108.545(3)	108.525(2)	108.612(2)
V (Å^3)	460.54(16)	459.33(7)	457.57(7)
Z	2	2	2
T (K)	193	193	193
λ (Å)	0.71073	0.71073	0.71073
ρ_{calcd} (g cm^{-3})	6.067	6.061	6.110
μ (cm^{-1})	349.71	342.64	348.32
R(F)[a]	0.0233	0.0330	0.0243
$R_w(F_o^2)$ [b]	0.0657	0.1104	0.0597

[a] $R(F) = \sum \left| |F_o| - |F_c| \right| / \sum |F_o|$ for $F_o^2 > 2\sigma(F_o^2)$. [b] $R_w\left(F_o^2\right) = \left[\sum \left[w\left(F_o^2 - F_c^2\right)^2 \right] / \sum wF_o^4 \right]^{1/2}$.

Table 2. Atomic Coordinates and Equivalent Isotropic Displacement Parameters for $Pr_{1.34}Yb_{2.66}S_6$.

Atom (site)	*x*	*y*	*z*	U_{eq} (Å^2)[a]
Pr1	0.55123(4)	0.25	0.19606(4)	0.00843(13)
Pr/Yb	0.18137(4)	0.25	0.00138(4)	0.01093(16)
Yb1	0.94227(3)	0.25	0.33496(3)	0.00997(13)
Yb2	0.65971(3)	0.25	0.58575(3)	0.01011(13)
S1	0.41859(19)	0.25	0.59374(19)	0.0086(4)
S2	0.8937(2)	0.25	0.5587(2)	0.0100(4)
S3	0.23343(19)	0.25	0.76947(19)	0.0090(4)
S4	0.3064(2)	0.25	0.25444(19)	0.0098(4)
S5	0.9805(2)	0.25	0.1160(2)	0.0121(4)
S6	0.61659(19)	0.25	0.96234(19)	0.0084(4)

[a] U_{eq} is defined as one-third of the trace of the orthogonalized U_{ij} tensor.

Table 3. Atomic Coordinates and Equivalent Isotropic Displacement Parameters for $PrTbYb_2S_6$.

Atom (site)	*x*	*y*	*z*	U_{eq} (Å^2)[a]
Pr1	0.55027(7)	0.25	0.19511(7)	0.0064(2)
Tb1	0.18125(6)	0.25	0.00196(6)	0.0075(2)
Yb1	0.94104(5)	0.25	0.33390(5)	0.0098(2)
Yb2	0.65988(5)	0.25	0.58556(5)	0.0096(2)
S1	0.4185(3)	0.25	0.5947(3)	0.0073(6)
S2	0.8943(3)	0.25	0.5591(3)	0.0085(6)
S3	0.2357(3)	0.25	0.7711(3)	0.0071(6)
S4	0.3064(3)	0.25	0.2532(3)	0.0095(6)
S5	0.9800(3)	0.25	0.1144(3)	0.0101(7)
S6	0.6159(3)	0.25	0.9625(3)	0.0081(6)

[a] U_{eq} is defined as one-third of the trace of the orthogonalized U_{ij} tensor.

Table 4. Atomic Coordinates and Equivalent Isotropic Displacement Parameters for $PrDyYb_2S_6$.

Atom (site)	*x*	*y*	*z*	U_{eq} (Å^2)[a]
Pr1	0.54996(5)	0.25	0.19506(5)	0.00797(13)
Dy1	0.18100(4)	0.25	0.00156(4)	0.00847(13)
Yb1	0.94108(4)	0.25	0.33369(4)	0.01048(13)
Yb2	0.66021(4)	0.25	0.58597(4)	0.01040(13)
S1	0.4181(2)	0.25	0.5945(2)	0.0087(5)
S2	0.8943(2)	0.25	0.5590(2)	0.0098(5)
S3	0.2348(2)	0.25	0.7715(2)	0.0088(4)
S4	0.3051(2)	0.25	0.2525(2)	0.0100(5)
S5	0.9799(2)	0.25	0.1140(2)	0.0101(5)
S6	0.6165(2)	0.25	0.9628(2)	0.0095(5)

[a] U_{eq} is defined as one-third of the trace of the orthogonalized U_{ij} tensor.

Table 5. Selected Bond Distances (Å) for $PrLnYb_2S_6$ (Ln = Pr/Yb, Tb, Dy).

Formula	$Pr_{1.34}Yb_{2.66}S_6$	$PrTbYb_2S_6$	$PrDyYb_2S_6$
Pr(1)-S(1) ×2	3.0127(16)	3.009(2)	3.0058(19)
Pr(1)-S(3) ×2	3.0068(16)	2.993(2)	3.0004(19)
Pr(1)-S(4)	2.958(2)	2.943(3)	2.947(3)
Pr(1)-S(6) ×2	2.8919(16)	2.877(2)	2.8755(19)
Pr(1)-S(6)	2.930(2)	2.919(3)	2.918(2)
Ln-S(3)	2.836(2)	2.837(3)	2.821(2)
Ln-S(4)	2.732(2)	2.715(3)	2.704(3)
Ln-S(5) ×2	2.7012(16)	2.692(2)	2.6832(18)
Ln-S(5)	2.881(2)	2.865(3)	2.863(2)
Ln-S(6) ×2	2.8977(15)	2.901(2)	2.8947(18)
Yb(1)- S(2) ×2	2.6819(15)	2.684(2)	2.6810(18)
Yb(1)-S(2)	2.726(2)	2.734(3)	2.731(2)
Yb(1)-S(3) ×2	2.7471(15)	2.752(2)	2.7426(18)
Yb(1)-S(5)	2.620(2)	2.630(3)	2.628(2)
Yb(2)-S(1) ×2	2.7557(15)	2.759(2)	2.7565(17)
Yb(2)-S(1)	2.673(2)	2.678(3)	2.680(2)
Yb(2)-S(2)	2.677(2)	2.675(3)	2.672(2)
Yb(2)-S(4) ×2	2.6134(14)	2.621(2)	2.6194(16)

Table 6. Magnetic Parameters for $PrLnYb_2S_6$ (Ln = Pr/Yb, Tb, Dy).

Formula	P_{cal}/μ_B	P_{eff}/μ_B	θ_p/K	R^2
$Pr_{1.34}Yb_{2.66}S_6$	8.48	7.91(1)	-36.9(8)	0.99979
$PrTbYb_2S_6$	12.19	11.82(1)	-3.1(4)	0.99992
$PrDyYb_2S_6$	12.92	11.38(2)	-0.2(7)	0.99979

[a] P_{cal} and P_{eff} : calculated [30] and experimental effective magnetic moments per formula unit.
[b] Weiss constant (θ_p) and goodness of fit (R^2) obtained from high temperature (100-300 K) data.

Figure Captions

Figure 1. An illustration of the three-dimensional structure of $PrTbYb_2S_6$ along the *b* axis.

Figure 2. Bicapped trigonal prismatic coordination environment of the Pr ions in $PrTbYb_2S_6$.

Figure 3. Inverse molar magnetic susceptibility plotted against temperature between 2 and 300 K for $Pr_{1.34}Yb_{2.66}S_6$. Data were taken under an applied magnetic field of 0.1 T. The straight line represents the fit to Curie-Weiss law in the range of 100-300 K.

Figure 4. The plot of the inverse molar magnetic susceptibility vs T for $PrTbYb_2S_6$ under an applied magnetic field of 0.1 T between 2 and 300 K. The straight line represents the fit to Curie-Weiss law in the range of 100-300 K.

Figure 5. The temperature dependence of the reciprocal molar magnetic susceptibility for $PrDyYb_2S_6$ under an applied magnetic field of 0.1 T between 2 and 300 K. The straight line represents the fit to Curie-Weiss law in the range of 100-300 K.

Figure 6. UV-vis diffuse reflectance spectra of $PrLnYb_2S_6$ (Ln = Pr/Yb, Tb, Dy).

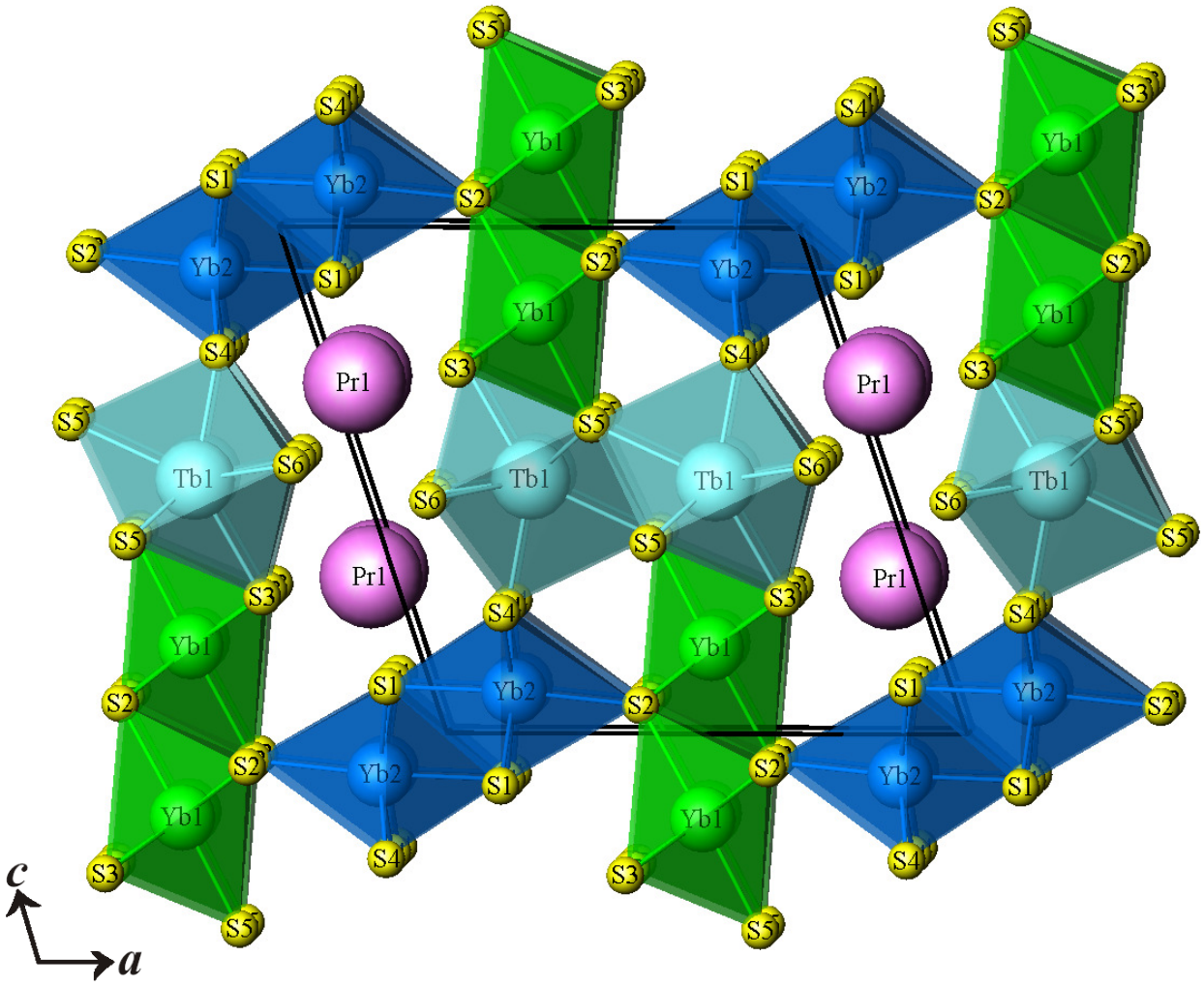
S5
S3
S4
Yb1
S1
Yb2
S2
S2
Yb2
S1
Yb1
S4
Pr1
S5
Tb1
S6
S5
Pr1
S3
Yb1
S2
S1
Yb2
S2
Yb2
S1
Yb1
S3
S4
S5
c
a

Figure 1

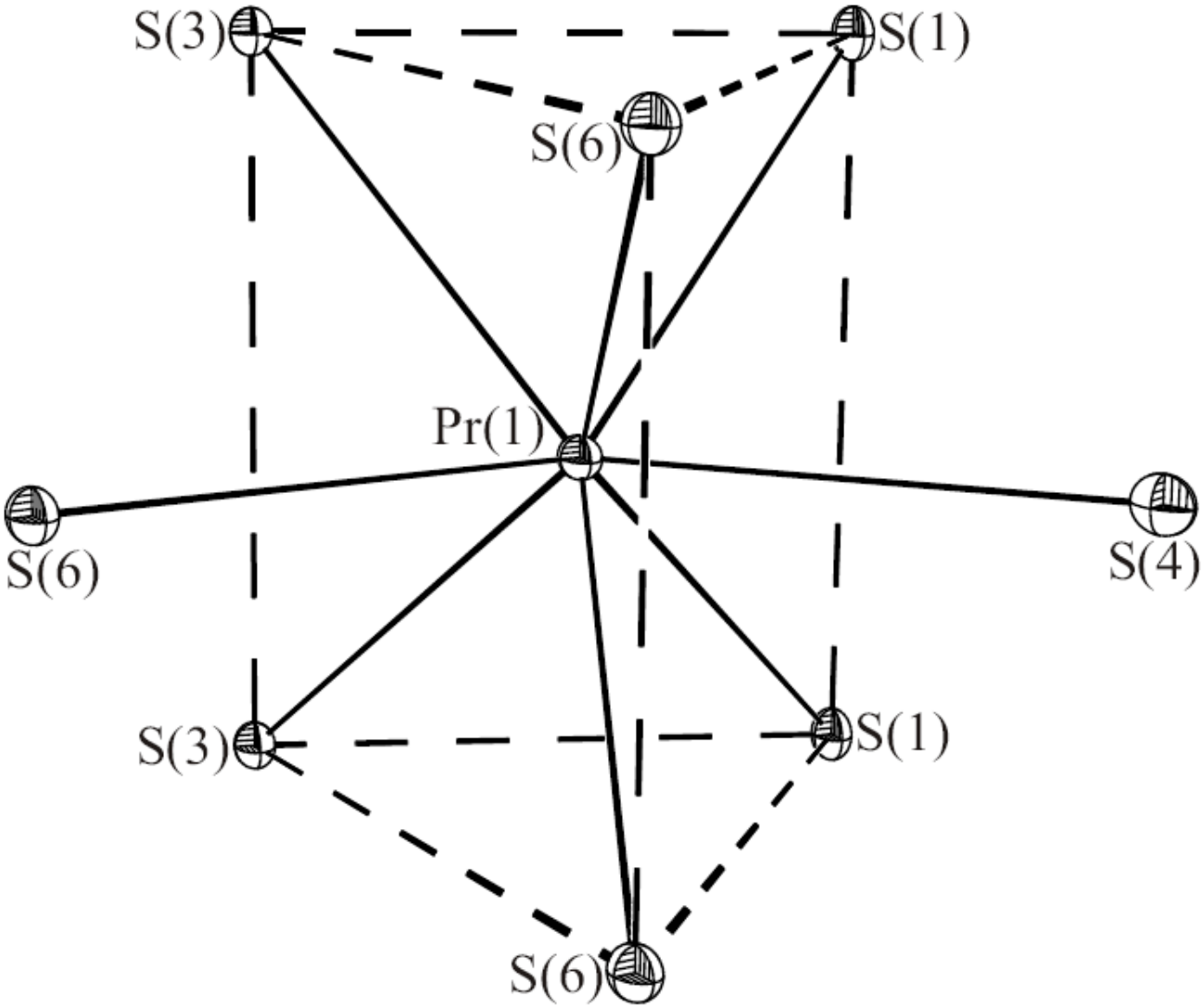

Figure 2

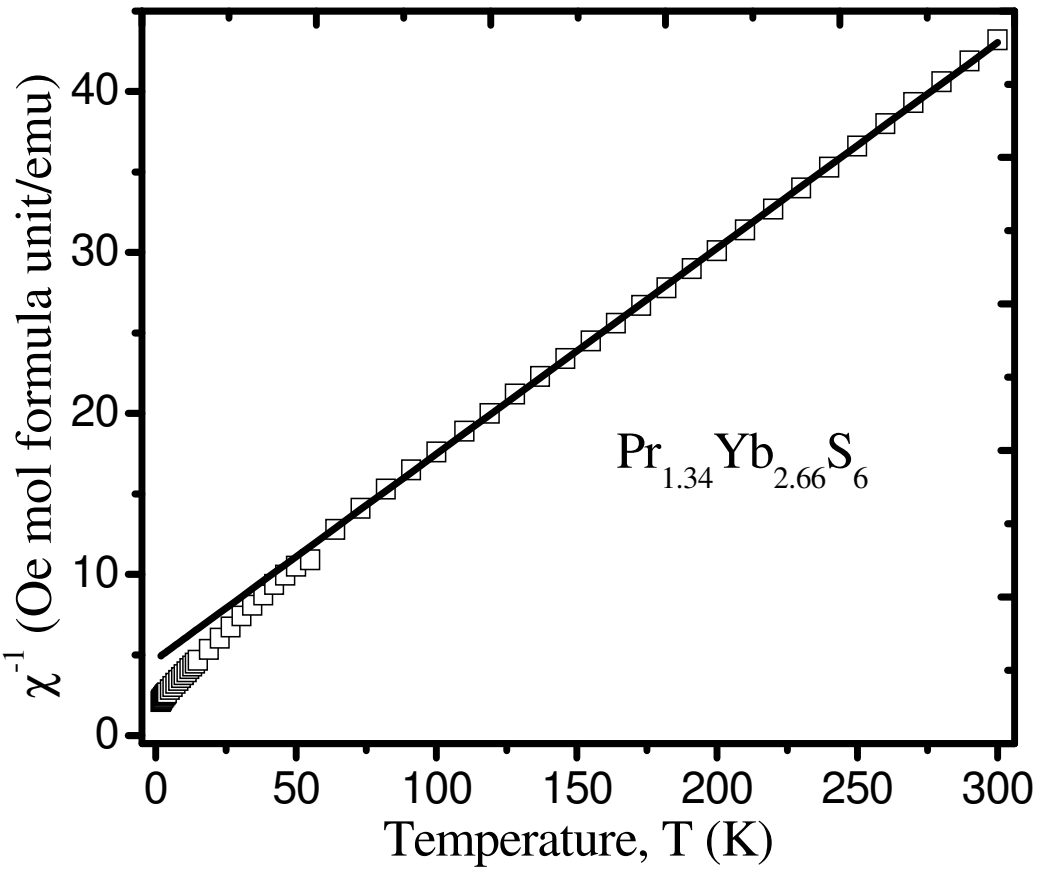
χ^{-1} (Oe mol formula unit/emu)
0
10
20
30
40
0
50
100
150
200
250
300
Temperature, T (K)
$Pr_{1.34}Yb_{2.66}S_6$

Figure 3

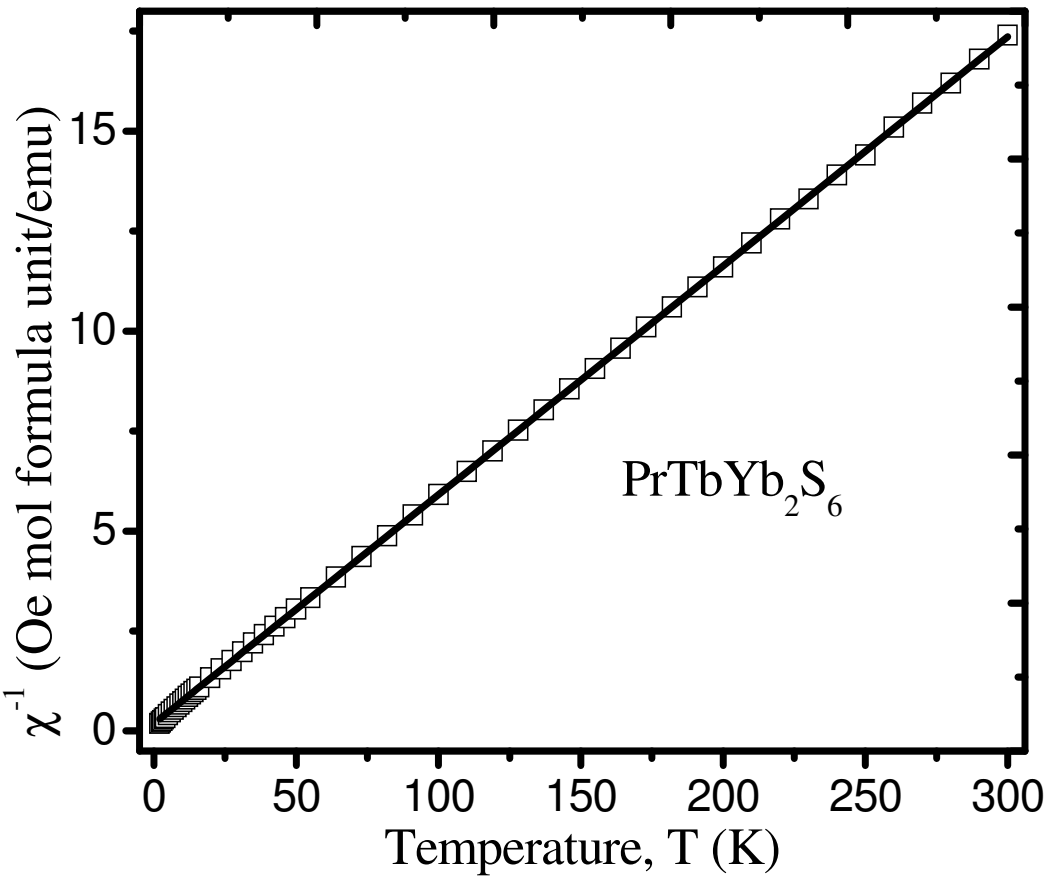
χ-1 (Oe mol formula unit/emu)
0
5
10
15
0
50
100
150
200
250
300
Temperature, T (K)
PrTbYb2S6

Figure 4

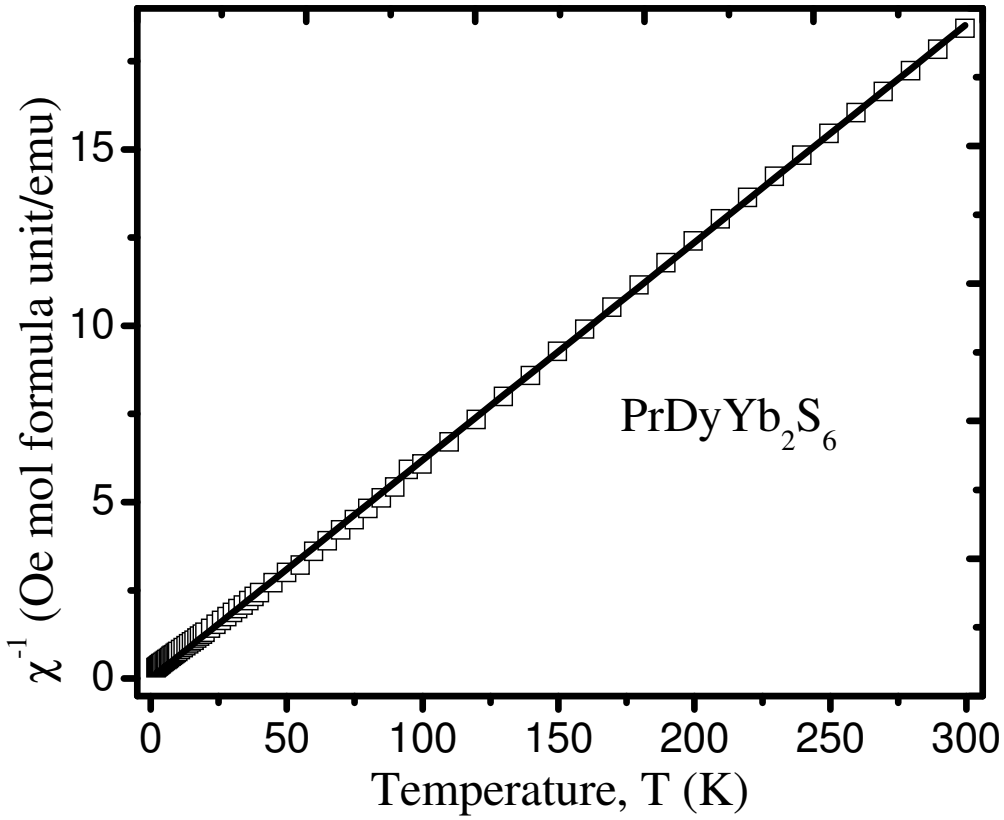
χ-1 (Oe mol formula unit/emu)
0
5
10
15
0
50
100
150
200
250
300
Temperature, T (K)
PrDyYb2S6

Figure 5

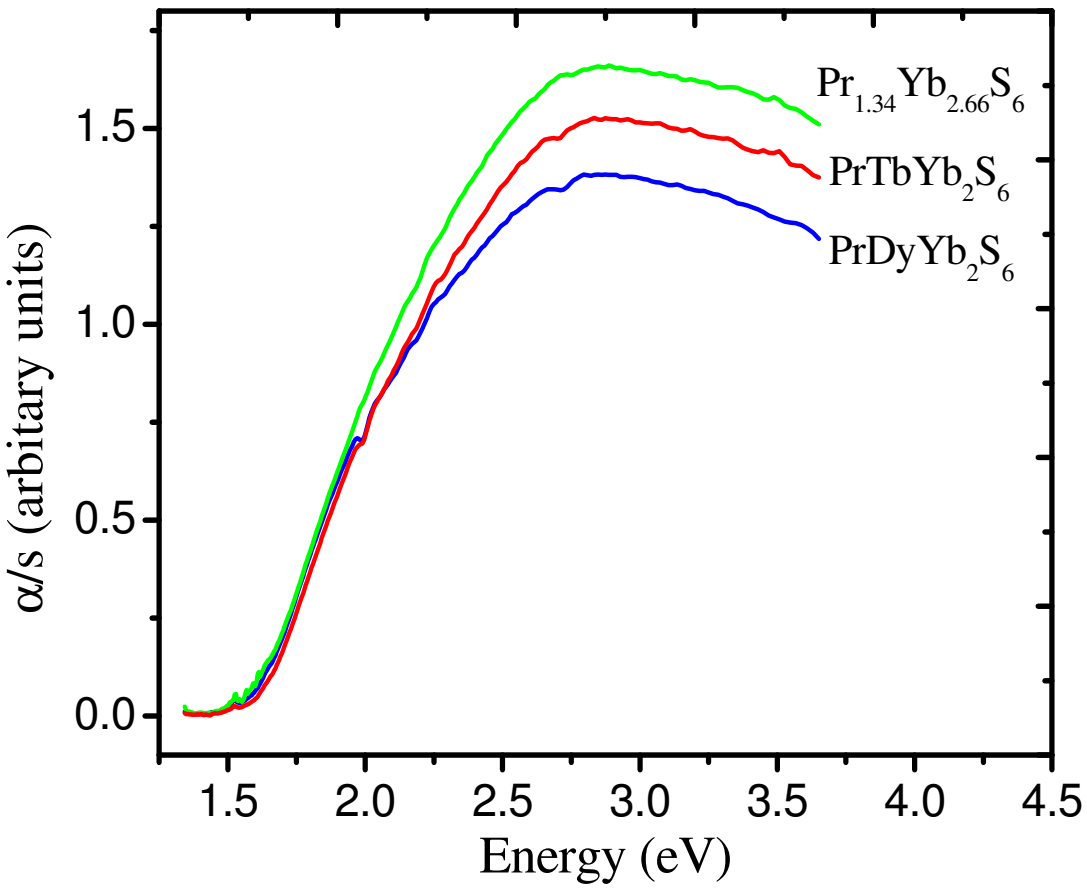
Pr1.34Yb2.66S6
PrTbYb2S6
PrDyYb2S6
α/s (arbitary units)
Energy (eV)
0.0
0.5
1.0
1.5
1.5
2.0
2.5
3.0
3.5
4.0
4.5

Figure 6